JOURNAL OF AIRCRAFT
Vol. 32, No. 1, January–February 1995

Response of a Nonrotating Rotor Blade to Lateral Turbulence Part II: Experiment

D. M. Tang* and E. H. Dowell†
Duke University, Durham, North Carolina 27706

In Part I of this work, a theoretical simulation study of rotor blade response to turbulence in forward flight is presented. For verification of this theoretical computational method, a new experimental method based on a special gust field generated by a rotating slotted cylinder with an airfoil (RSC/airfoil) in a wind tunnel is developed to simulate the aerodynamic environment of a rotating rotor blade in forward flight. This gust generator can produce a single harmonic gust wave and also turbulence with uniform power spectral density over a certain frequency band in the lateral and longitudinal directions. In this article, quantitative comparisons are also made with theoretical results for both random and nonrandom parametric excitation. The quantitative agreement between theory and experiment indicates that this experimental method is useful.

Nomenclature

C = airfoil chord
$|C_{L1}|$ = magnitude of dynamic lift coefficient
k = reduced frequency, $\omega C/2u_0$
$L, \bar{L}$ = longitudinal position from cylinder centerline, L/C
U = resultant longitudinal flow velocity
u_G = resultant longitudinal gust velocity
u_s = longitudinal sinusoidal pulsating velocity
u_η = longitudinal turbulence velocity
u_0 = constant freestream velocity
w_G = resultant lateral gust velocity
w_s = lateral sinusoidal gust velocity
w_γ = lateral turbulence velocity
$y, \bar{y}$ = lateral position from tunnel centerline, y/C
$y_0, \bar{y}_0$ = distance between adjacent cylinders, y_0/C
α_G = gust angle of attack, w_G/u_0
Γ = vortex strength
ψ_d = dynamic phase difference between adjacent cylinders
ω_s = cylinder rotation speed

I. Introduction

IN Part 1 of this work,[8] a theoretical simulation study of rotor blade response to turbulence in forward flight is presented. To understand the fundamental physics of the parametric random vibration of a helicopter rotor blade, an experimental investigation is very important, not only to verify the theoretical results, but also to explore response characteristics not predicted by the available analytical methods.

During the past several years, a few correlation studies have compared theoretical results with those from wind-tunnel experiments and flight tests. In Ref. 1 a periodic mean square flapping response of a rotor blade model was measured in a wind tunnel by applying a random perturbation generated by a turbulent grid before the experimental model. The rotor model with three blades only provided for flapping motion. The flap angle and azimuth position measurements in this rotating system use a multiple channel slip ring assembly and phototransistor. This apparatus affected the measurement accuracy of the flapping response variance. The test results were also used to verify a theoretical model using the direct time domain approach as shown in Ref. 2. The flapping autocorrelation measurement for an articulated rotor blade,[3] and the experimental time-averaged power spectra of a V/STOL propeller blade, as well as the wing response of hingeless and gimballed rotor-propeller configurations, have been presented in Refs. 4 and 5. These tests support the validity of some theoretical concepts, but did not evaluate the accuracy of the approximate computational methods.

In this article, a new experimental design differing from the conventional wind-tunnel test of a rotor blade is described. The blade model is nonrotating. The aerodynamic effects due to the rotating speed relative to the blade are simulated by a special flowfield with a sinusoidal pulsating stream and lateral turbulence in the wind tunnel. We assume the atmospheric turbulence to be homogeneous and isotropic, and the effects of self-induced turbulence by the lifting surface, such as downwash and trailing vortices, to be negligible. The differential equations describing this experimental system are very similar to those of a rotor blade in forward flight. The response statistics vs azimuth angle of the rotor blade are determined by a controllable field parameter. This experimental configuration has several advantages, including convenience and low cost for the gust test of a rotor blade in a wind-tunnel environment.

The experimental results presented in this article are compared with those calculated from a direct time domain method using a modified linear ONERA aerodynamic model. The quantitative agreement between theory and experiment indicates that this experimental method is useful.

II. Experimental Simulation for Gust Excitation

Unlike the usual rotor experimental model in a wind tunnel, a cantilevered nonrotating flexible blade with NACA 0012 airfoil shape is used here as the experimental model. In order to simulate parametric random vibration motion of the rotor blade of rotorcraft in forward flight (i.e., a differential equations of motion simulation rather than a physical simulation of the practical rotorcraft per se), the wind-tunnel environment is especially designed. A dominant lateral turbulence velocity component and a lateral sinusoidal velocity component that are normal to the blade plane, and a dominant longitudinal sinusoidal velocity component with a longitudinal turbulence are generated by a combined rotating slotted cylinder and airfoil system (RSC/airfoil). A simplified aerody-

Received Aug. 31, 1993; revision received Feb. 18, 1994; accepted for publication May 3, 1994.

*Research Associate, Department of Mechanical Engineering and Materials Science.
†Dean, School of Engineering, Department of Mechanical Engineering and Materials Science.

namic theory for this gust generator system is described as follows.

An analysis was made of a simple conceptual mathematical model for a two-RSC/airfoil gust generator system (Fig. 1). This analysis follows that of Reed.[6] For simplicity, the flowfield is assumed to be quasisteady, i.e., k is small, and wind-tunnel wall effects are neglected. The problem, then, is to determine the magnitude of the gust velocities induced at a point in this gust flowfield. Take the coordinates of the space point p in the XYZ coordinate system as x_p, y_p, and z_p as shown in Fig. 1. The lift generated by each airfoil is approximately represented by a linear segment vortex of strength Γ located at the quarter-chord of the RSC/airfoil system. The Biot-Savart law is used to determine the gust flowfield induced by these linear segment vortices. In vector notation, the elementary velocity $d\boldsymbol{v}$ induced at the point p by an element $d\boldsymbol{s}$ belonging to the line vortex of strength Γ is expressed as follows:

$$d\boldsymbol{v} = \frac{\Gamma}{4\pi}\frac{d\boldsymbol{s} \times \boldsymbol{l}}{l^3}$$

The total induced velocity $\boldsymbol{v}$ at that point becomes

$$\boldsymbol{v} = \frac{\Gamma}{4\pi}\int_c \frac{d\boldsymbol{s} \times \boldsymbol{l}}{l^3}$$

As shown in Fig. 1, the plane velocity vector $\boldsymbol{v}_2$, induced by the line vortex of strength Γ_2 can be represented by

$$\boldsymbol{v}_2 = \left(\frac{\Gamma_2}{2\pi R_2}\right)$$

where

$$R_2 = \sqrt{x_p^2 + (y_0 - y_p)^2}$$

The magnitude of the lateral and longitudinal gust velocities v_{2y} and v_{2x} are

$$v_{2y} = v_2\frac{x_p}{R_2}, \qquad v_{2x} = -v_2\frac{y_0 - y_p}{R_2}$$

Similar to above derivation, the velocity vector $\boldsymbol{v}_1$ at the same p induced by Γ_1 can also be obtained. The resultant

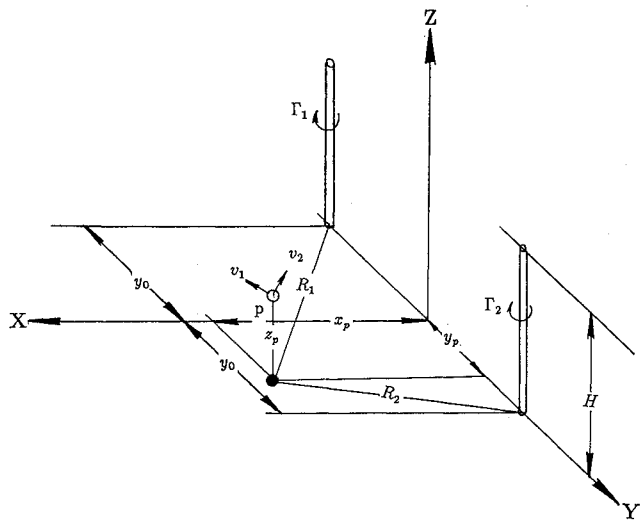

Fig. 1 Simple theoretical aerodynamic model.

lateral w_G and longitudinal u_G gust velocities induced at that point by each of the two vortices are

$$w_G = v_{1y} + v_{2y} = \frac{x_p}{2\pi}\left(\frac{\Gamma_1}{R_1^2} + \frac{\Gamma_2}{R_2^2}\right) \tag{1}$$

$$u_G = v_{1x} + v_{2x} = \frac{1}{2\pi}\left[\frac{\Gamma_1(y_0 + y_p)}{R_1^2} - \frac{\Gamma_2(y_0 - y_p)}{R_2^2}\right] \tag{2}$$

where

$$R_1 = \sqrt{x_p^2 + (y_0 + y_p)^2}$$

The vortex strength and the lift coefficient for a two-dimensional airfoil are related by the equation:

$$\Gamma = \tfrac{1}{2}C_L u_0 C$$

If there is a phase difference, $\psi_d = \psi_1 - \psi_2$ between two cylinders (ψ_1, ψ_2 are the initial phase angle of the cylinders), then the lift coefficients for the two distinct airfoils in the cascade can be represented approximately as follows[9]:

$$\begin{aligned} C_{L1} &= 0.5C(k)\sin 2\omega_s t \\ C_{L2} &= 0.5C(k)\sin 2(n\omega_s t + \psi_d) \end{aligned} \tag{3}$$

where $C(k)$ is Theodorsen's function, and n denotes the rotational speed ratio of cylinder 1 to cylinder 2. The use of $C(k)$ to modify the steady flow relations is consistent with our quasisteady assumption made earlier.

The lateral and longitudinal gust velocities are given by

$$\frac{w_G}{u_0} = \frac{0.5C(k)\bar{x}_p}{4\pi}\left[\frac{1}{\bar{R}_1^2}\sin 2\omega_s t + \frac{1}{\bar{R}_2^2}\sin 2(n\omega_s t + \psi_d)\right] \tag{4}$$

$$\frac{u_G}{u_0} = \frac{0.5C(k)}{4\pi}\left[\frac{(\bar{y}_0 + \bar{y}_p)}{\bar{R}_1^2}\sin 2\omega_s t - \frac{(\bar{y}_0 - \bar{y}_p)}{\bar{R}_2^2}\sin 2(n\omega_s t + \psi_d)\right] \tag{5}$$

where the bar superscript denotes distance in chord units, and $2\omega_s$ and $2n\omega_s$ are the gust frequencies. The magnitude of gust intensity can be varied by changing the phase difference ψ_d.

When $y_p = 0$, $\psi_d = 0$, and $n = 1$, i.e., p is located on the centerline of the wind-tunnel test section, and there is a single rotating speed and the same rotating direction for the two cylinders, we have

$$\frac{u_G}{u_0} = 0$$

$$\alpha_g = \frac{u_G}{u_0} = \frac{0.5C(k)}{2\pi}\frac{\bar{x}_p}{\bar{R}_1^2}\sin 2\omega_s t$$

When $n = -1$, i.e., there is a single rotating speed and counter-rotating directions for the two cylinders, we have

$$\frac{u_G}{u_0} = \frac{0.5C(k)}{2\pi}\frac{\bar{y}_0}{\bar{R}_1^2}\sin 2\omega_s t$$

$$\alpha_g = \frac{u_G}{u_0} = 0$$

When the cylinder rotational speed is a continuous linear frequency sweep speed from ω_1 to ω_2 in a sweep duration T, we can obtain a continuous frequency sweep lateral or longitudinal gust with nearly uniformly distributed power spectral

density in a specific frequency. We use this kind of gust to simulate atmospheric turbulence in this article. The turbulence is homogeneous and isotropic over the whole span of the blade model, and has a uniform power spectral density over the fundamental blade response frequency band.

There are four RSC/airfoils placed at the wind-tunnel test section entrance (see Fig. 2). As shown in Fig. 2, the no. 2 and no. 3 RSC/vanes are symmetrical relative to the centerline of the tunnel. The rotating direction of cylinder no. 2 is anticlockwise, whereas that of cylinder no. 3 is clockwise. Together they produce longitudinal and lateral sinusoidal (ψ_d = 0) gust components with amplitudes u_s and u_0, at any position behind the RSC/airfoils. The no. 1 and no. 4 cylinders have the same rotational direction with a variable rotor speed, $\omega t^r/T$ (if $\varepsilon = 1$, it is a linear frequency sweep). The gust flowfield behind the no. 1 and no. 4 RSC/airfoils includes lateral and longitudinal turbulence.

If the nonrotating blade model is placed at $p(x_p, y_p)$, as shown in Fig. 2, the resultant longitudinal and lateral gust components for $\psi_d = 0$ are given by

$$u_G = u_s \sin \Omega t + u_\eta \tag{6}$$

$$w_G = w_s \sin \Omega t + w_\gamma \tag{7}$$

where $\Omega = 2\omega_s$, u_η, and w_γ are the longitudinal and lateral turbulent components.

When p is placed in the symmetrical plane of the wind tunnel, i.e., $y_p = 0$, then $u_\eta = 0$, $u_G = u_s \sin \Omega t$ and $w_G = w_\gamma$ has its maximum lateral gust strength.

III. Experimental Methods for Measuring Response Statistics of a Flexible Blade

The experiments were performed in the Duke University low-speed wind tunnel. The wind tunnel is a closed circuit tunnel with a test cross section of 2.3 × 1.75 ft², and a length of 5 ft. The maximum air speed attainable is 293 ft/s. The wind-tunnel test blade model, response measurement, excitation, and data analysis systems are discussed as follows.

A. Experimental Model

The experimental model includes two parts: 1) a nonrotating rotor blade section and 2) a root support mechanism.

The blade model is rectangular in planform, untwisted and flexible in the flap and torsional directions. The blade is constructed from a flexible aluminum beam with eight light wood styrofoam fairing elements covering the entire chord and span that provide the aerodynamic contour of the blade. Each element is attached to the spar independently so that the stiffness of the spars would not be altered. The gap between two neighboring elements is covered by a piece of adhesive tape that allows the blade to be flexible in both the bending and torsional directions.

The root mechanism is mounted to a very heavy support frame that is attached to the ground. The pitch axis of the blade is supported on upper and lower bearings in a blade root socket and is free to move in the pitch direction. The pitch spring uses a steel wire spring material. The steel wire is inserted tightly into a slot of the blade root socket. The support at the end of pitch spring is allowed to have rotation and slip motions without transverse motion. The pitch natural frequencies can be adjusted by moving the support position of the pitch spring. The effective mean pitch angle can be adjusted by rotating the root support mechanism. All parameters of the model are summarized in Table 1.

B. Response Measurement System

Strain gauges were used for measurement of flap and elastic torsional deflections. An axial gauge (flap) for bending modes and a 45-deg gauge for torsional modes were glued to the flexible rotor blade spar to measure the bending-torsional deflections of the blade tip. Signals from the strain gauges were conditioned and amplified before their measurement through a low-pass filter. The pitch angular displacements at the blade root were measured by a rotational velocity/displacement transducer, RVDT. The output signals from these strain gauges and transducers were amplified and directly recorded on a MacIntosh IIci computer through a data acquisition package, NB-MIO-16, which consisted of a 16-channel analog to digital (A/D) plug-in interface board, a BNC ter-

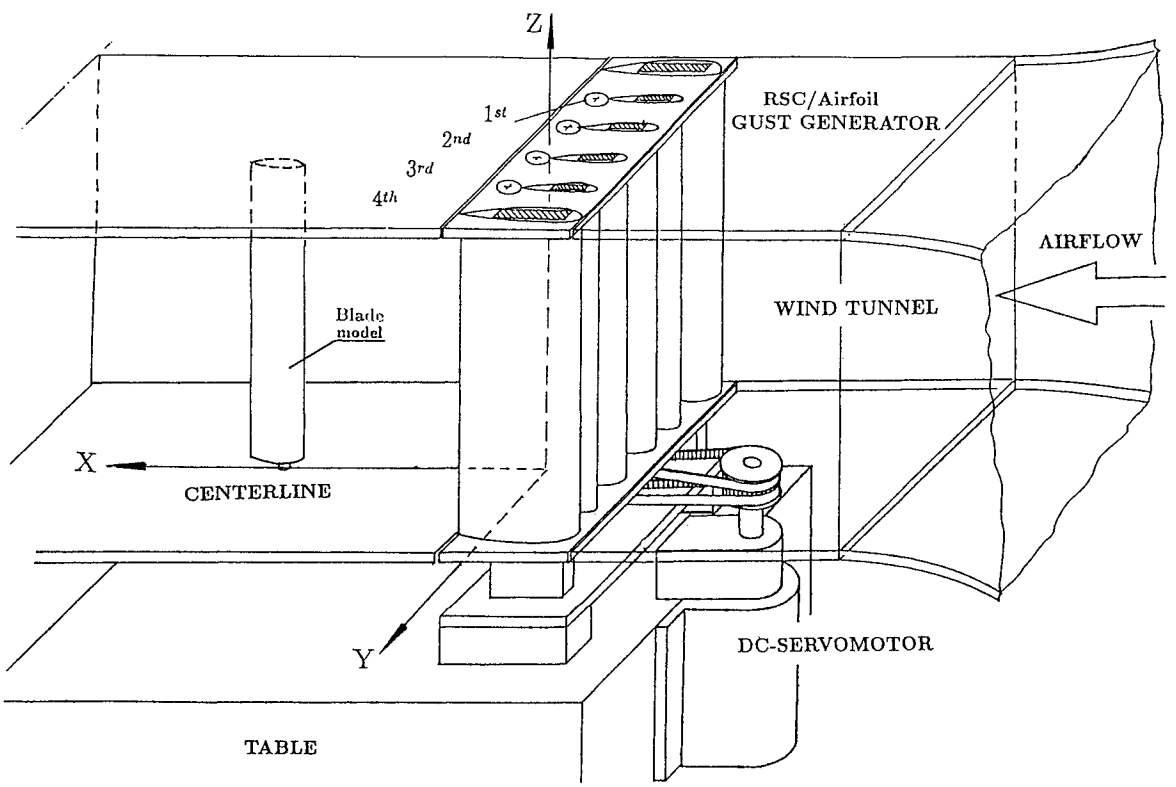

Fig. 2 Sketch of the configuration for the RSC/airfoils.

Table 1 Model parameters

R	19.68, in.
b	1.57, in.
ω_z	10, Hz
ω_y	17.8, Hz
GJ	0.25×10^4, lb/in.^{2}
m	0.47×10^{-4}, lb^2/in.^{2}
K_m	1.149, in.
$K_{\phi s}$	18.62, lb/in./rad
e	0.315, in.
ab	−0.63, in.

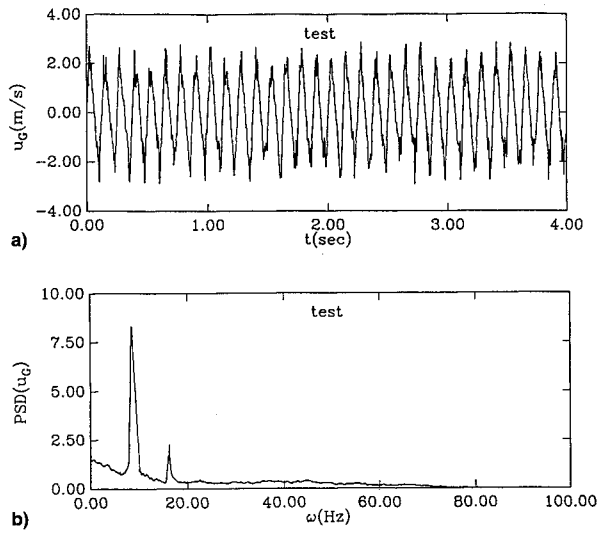

Fig. 3 Measured longitudinal gust generated by a ω_s = 4-Hz rotation of RCS no. 2 and no. 3 for u_0 = 23 m/s, y_p = 0: a) time history and b) PSD plot.

mination box, and data acquisition and analysis software, LabVIEW. The digitized response data could be used to determine response statistical quantities. In order to obtain a comparison of the theory with the test, a measurement system calibration was completed before the wind-tunnel test. The dynamic calibration coefficients were determined by a ground vibration test. The dynamic calibration assumed that there was no significant coupling between the bending and torsional directions. This is a reasonable assumption for the present test configuration.

In order to provide precisely the gust field data for theoretically calculating the flapping and torsional response vs the azimuth angle in this experimental model, a set of lateral and longitudinal differential pressure probes is placed at the aerodynamic center axis of the blade model and at the midheight of the tunnel. The gust field measurement is carried out before the response measurement of the blade model, and test conditions must remain identical for the two measurements. There is a technical difficulty in synchronizing the gust excitation signals and the blade responses at the special position of the blade aerodynamic center axis for the present test model. However, this does not affect the theoretical and experimental results because the gust field is a stationary and continuously random or periodic process.

C. Excitation System Control

As discussed in Sec. II, the no. 2 and no. 3 RSC/vanes are used to generate the sinusoidal longitudinal gust, whereas the no. 1 and no. 4 RSC/vanes are used to generate a lateral frequency sweep gust. The two pairs of gust generators are controlled by a 2-channel digital to analog (D/A) plug-in interface board in a Macintosh IIci computer. The control execution software is written in the LabVIEW environment. A typical measured longitudinal gust wave is shown in Fig. 3a. The airstream velocity and cylinder rotation speed are U = 23 m/s, and ω_s = 4 Hz, respectively. The pressure probes are placed at L = 6 in. from the cylinder center in the horizontal direction, y_p = 0 in the lateral direction, and H = 10.5 in. from the bottom of the tunnel in the vertical direction. A corresponding power spectral density (PSD) plot is shown in Fig. 3b. It is found that the dominant signal is a single sine-wave, with a detectable second harmonic component. Background noise due to the shed vortices behind the rotating cylinders is also present, but is not very strong.

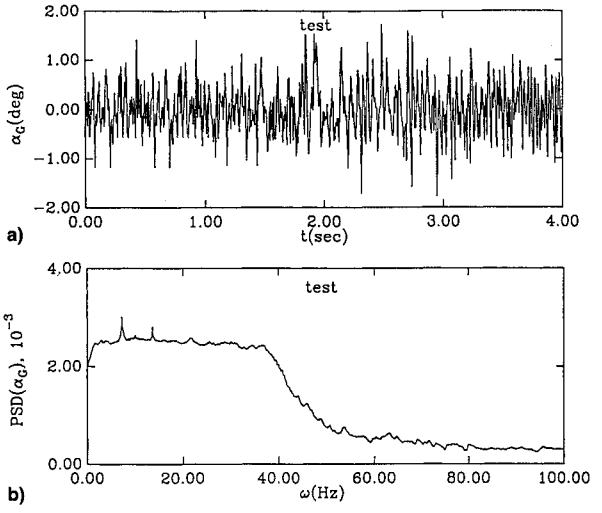

Fig. 4 Measured lateral gust generated by linear frequency sweep of RCS no. 1 and no. 4 for u_0 = 23 m/s, y_p = 0: a) time history and b) PSD plot.

Figure 4a shows a typical measured lateral gust wave generated by the linear frequency sweep of RCS no. 1 and no. 4 for an airstream velocity of U = 23 m/s, and cylinder rotation speeds from 0 to 20 Hz in 2.8 s. A corresponding power spectra plot is shown in Fig. 4b. A relatively uniform power spectral density in the 0–40-Hz frequency band is obtained. Also, small first and second harmonic components arising from the no. 2 and no. 3 RSC/airfoils are present in the lateral gust.

D. Autocorrelation Response Evaluation

There are various methods to determine the response autocorrelation function or variance response of a blade.

1. Measuring Time-Varying Frequency Response Functions

For a given longitudinal gust frequency, we measure the steady frequency response function of the blade model generated by the no. 1 and no. 4 RSC/airfoils using a harmonic gust excitation. From a large sampling of measurement data, we take an ensemble average, and obtain a frequency response curve $H_s(\omega_i, t)$ for one cycle (one revolution of the sinusoidal longitudinal wave). Then the data are stored in the computer and normalized by the sine gust excitation amplitude. The $H_c(\omega_i, t)$ is obtained by shifting $\pi/2$ in phase from the original frequency response curve. Changing the lateral gust frequency, we obtain a family of frequency response curves. From the known excitation PSD, $\sigma_{\alpha i}(\omega_i)$ is determined. The total time variable variance of the blade response is determined by summation of the individual variances.

2. Measuring the Time History of the Response Under Frequency Sweep Excitation

For a given longitudinal gust frequency, we directly measure the time histories of flapping, torsional motions, and the longitudinal gust sine wave under the continual frequency sweep excitation generated by the no. 1 and no. 4 RSC/airfoils. For two specific azimuth angles of the reference rotating sine signal, e.g., ψ_1 and ψ_2, each pair of flapping responses

w corresponding to ψ_1 and ψ_2, is taken consecutively to form a product, i.e.,

$$\langle w_K(\psi_1) w_K(\psi_2) \rangle_K$$

where K is the sampling number. When the ψ_1 and ψ_2 are continually lagged for one revolution of the sine longitudinal wave, the autocorrelation function of blade response with the time lag $\psi_2 - \psi_1$, is obtained. If the time lag is zero, a measured time variable variance of the blade response is determined.

This method is applied in the present experiment to determine the time variable variance response over a one cycle. The sampling rate is 800 points/s and the fundamental excitation frequency for the longitudinal gust is 8 Hz. Total sample time is taken as 15 s after a steady-state blade motion is reached. The measured flap response time series is represented as

$$w_0(t_0),\ w_1(t_0 + \Delta t),\ w_2(t_0 + 2\Delta t),\ \ldots,\ w_k(t_0 + k\Delta t)$$

where t_0 is the measurement start time (here, assuming $t_0 = 0$), $\Delta t = 1/800$ s and $k = 12{,}000$.

Taking the first data point, e.g., $n_p = 1$, as a reference position (or azimuth angle $\psi_1 = 0$) and $\psi_1 = \psi_2$, the flap autocorrelation function at the zero time lag in a one cycle ($\psi = 0$–2π or $n_p = 1$–100) is determined from the above measured flap response time series. It is given by

$$\sigma_w^2(\psi) = \frac{1}{120} \sum_{j=1}^{120} w^2[100(j-1) + n_p]$$

The torsional autocorrelation function is

$$\sigma_\phi^2(\psi) = \frac{1}{120} \sum_{j=1}^{120} \phi^2[100(j-1) + n_p]$$

where $w[..]$, $\phi[..]$ are the digitized values of the response time series corresponding to 1–12,000 response data points.

IV. Theoretical and Experimental Correlation

Theoretical calculations are based on a direct time simulation method (see Part I of this work), and the measured longitudinal and lateral gust time histories α_G and u_G. The theoretical longitudinal gust representation also includes a time derivative of u_G. However, in the wind-tunnel test, only u_G is recorded, therefore, to get the term $\dot{u}_G$ requires differentiation. The differentiation process will amplify the high-frequency noise and attenuate the low-frequency signal. To alleviate this problem Takens[7] proposed a method for constructing a phase plane plot in a nonlinear dynamical system using fake observables generated from a single experimental measurement. In this method for forming fake observables, an important parameter is the embedding time. It depends upon the system dynamics. For a dominant single periodic measured signal, a good choice is about one-quarter of the period. As shown in Fig. 3b, the 8-Hz component is much stronger than the other components and, hence, there is a dominant frequency of oscillation. An embedding time of 25 samples is used throughout this article. This is based on a data sampling rate of 800 points/s, and a quarter of the dominant oscillation period $\frac{1}{32}$ s. Therefore, we can obtain velocity digitized values $\dot{u}_G[..]$ from the original measured longitudinal gust digitized values $u_G[..]$, using 25 lagging samples and multiplying by the dominant oscillation frequency in the original u_G series. The principal advantage of Takens' method is that it eliminates the need for differentiation of the measured signal.

Two cases are used for the theoretical and experimental correlation. One is when the blade model is placed in the symmetrical plane of the wind tunnel, i.e., $y_p = 0$. This is to simulate the nonrandom parametric excitation case. Another case is for $y_p = 2$ in., which is used to simulate the random parametric excitation case.

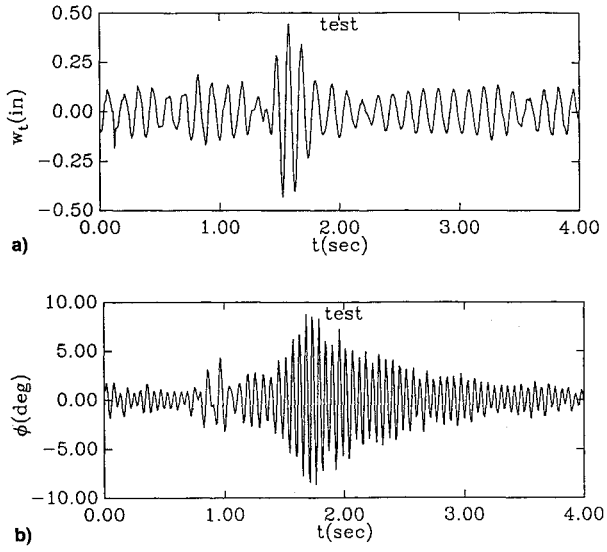

Fig. 5 Measured response time history for $u_0 = 23$ m/s, $y_p = 0$, $\theta_0 = 0$: a) flap and b) torsional responses.

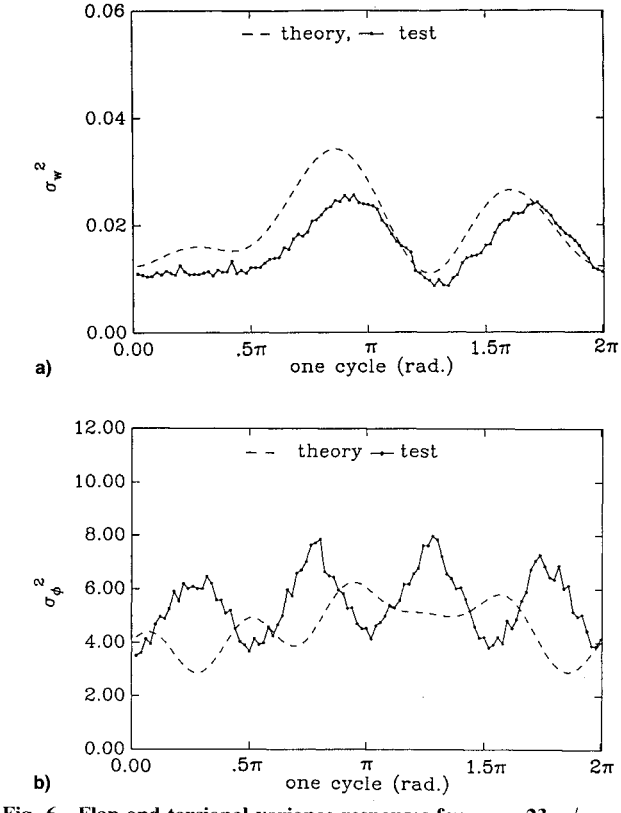

Fig. 6 Flap and torsional variance responses for $u_0 = 23$ m/s, $y_p = 0$, $\theta_0 = 0$, for a) flap and b) torsional variance response σ_ϕ^2 vs ψ.

A. Nonrandom Parametric Excitation Case

In this case we have $y_p = 0$ and $u_\eta = 0$. Figure 5 shows the measured flap and torsional responses under a given gust flow for $u_0 = 23$ m/s, $\Omega = 8$ Hz, and $\theta_0 = 0$. The measured gust excitations are shown in Figs. 3 and 4. As shown in Fig. 5a, the flap response is dominated by the 8-Hz excitation frequency component. In each 3.7 s, there is a burst of response amplitude. This is because the lateral gust is due to a continuous linear frequency sweep gust with a 3.7-s period (including a 0.9-s time delay because of the rotational inertia of the dc-motor). For the torsional response, the motion is

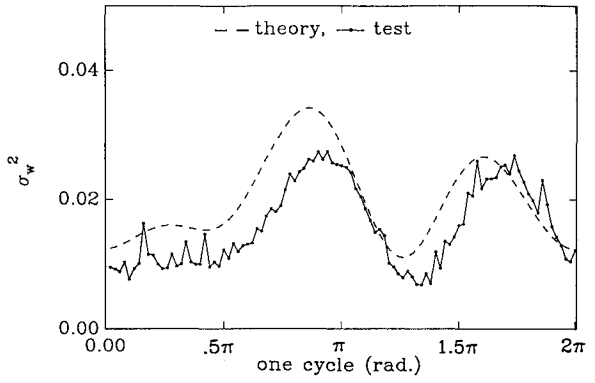

Fig. 7 Flap variance response for $u_0 = 23$ m/s, $y_p = 0$, $\theta_0 = 5$ deg.

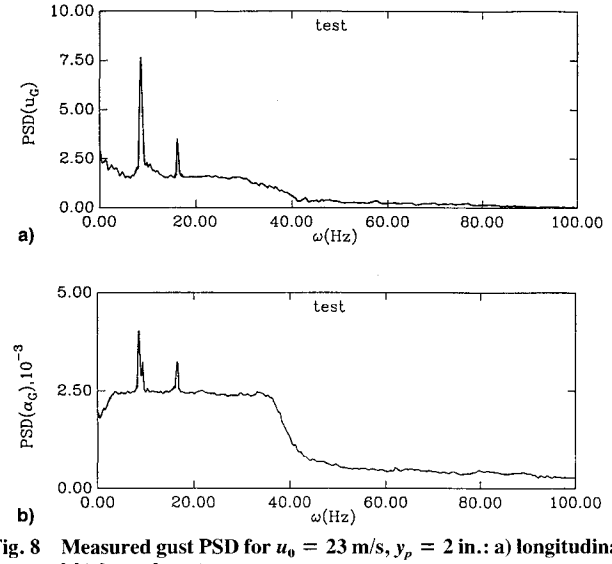

Fig. 8 Measured gust PSD for $u_0 = 23$ m/s, $y_p = 2$ in.: a) longitudinal gust and b) lateral gust.

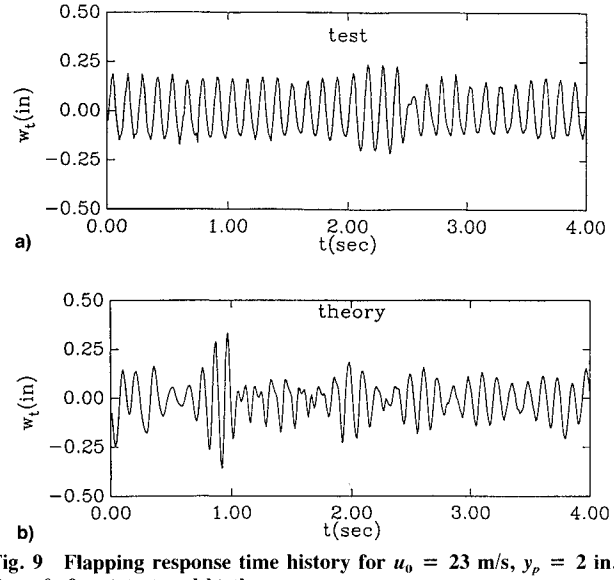

Fig. 9 Flapping response time history for $u_0 = 23$ m/s, $y_p = 2$ in., $\theta_0 = 0$, for a) test and b) theory.

dominated by the 17.8-Hz oscillation frequency (the first torsional natural frequency) component as shown in Fig. 5b. This is because the torsional response is quite sensitive to α_G, which has a uniformly distributed power spectral density between 0–40 Hz. The response wave is similar to a free oscillation with a single oscillation frequency under a continuous frequency sweep excitation. The torsional response is weakly influenced by the 8-Hz longitudinal gust component.

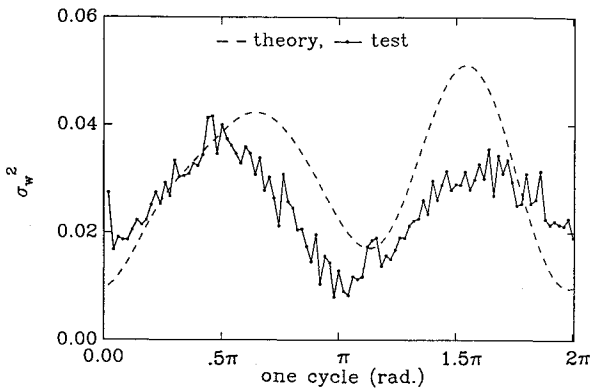

Fig. 10 Flap variance response for $u_0 = 23$ m/s, $y_p = 2$ in., $\theta_0 = 0$ deg.

Figure 6 shows the measured flap and torsional variance responses for the same condition as the above. As shown in Fig. 6a, the flap variance has two peaks in one cycle. This is because the oscillation frequency of the flap response is dominated by the 8-Hz frequency component. For the torsional variance response, there are four peaks in one cycle as shown in Fig. 6b. This is because the oscillation frequency of the torsional response is dominated by the 17.8-Hz frequency component. For comparison of the theoretical and experimental results, the theoretical results are also plotted in the same figures as indicated by the dashed line in Fig. 6. The agreement between theory and experiment is fair to good.

Figure 7 shows the experimental and theoretical flap variance responses for the same condition as the above, but now $\theta_0 = 5$ deg. The agreement is also reasonably good. Comparing this figure to Fig. 6a, the flap variance response magnitude increases as θ_0 increases both for the theoretical and experimental results, but the increment is slight. For the torsional variance response (not shown), the result is similar to Fig. 6b.

B. Random Parametric Excitation Case

In this case, we have $y_p = 2$ in. and $u_\eta \neq 0$. The measured input gust PSD plots are shown in Figs. 8a and 8b. Note that due to $y_p \neq 0$, each rotating cylinder can produce both longitudinal and lateral gusts, but the quantitative contribution is different. Comparing Figs. 8a and 8b to Figs. 3b and 4b, we find that for the u_G signal the gust component of the continual frequency sweep excitation generated by the no. 1 and no. 4 RSC/vanes is added to the longitudinal gust. The second harmonic frequency component (16 Hz) and the background white noise slightly increase, and the dominant frequency component (8 Hz) slightly decreases. For the α_G signal, the 8-Hz and 16-Hz frequency components generated by the no. 2 and no. 3 RSC/vanes are added to the lateral gust. The variations of the background noise and frequency sweep gust components are small.

Figure 9a shows measured flap response under a given gust flow for $u_0 = 23$ m/s, $\Omega = 8$ Hz and $\theta_0 = 0$. A more sinusoidal wave with an 8-Hz frequency is obtained and the burst in amplitude is attenuated compared to Fig. 5a. A theoretical flap response is also shown in Fig. 9b. The theoretical result has more harmonic frequency components than the experimental data. The theoretical and experimental flapping variance responses are shown in Fig. 10. The variance magnitude is larger as compared to the nonrandom parametric excitation case. This is because, firstly, the longitudinal turbulence is enhanced, and secondly, the 8-Hz harmonic component in the lateral gust becomes stronger. The latter may be more significant than the former.

Figure 11 shows the flapping and torsional variance responses for $\theta = 5$ deg, and without changing other conditions. The response amplitude for both flapping and torsional motions increases as compared to Fig. 10. Especially, comparing

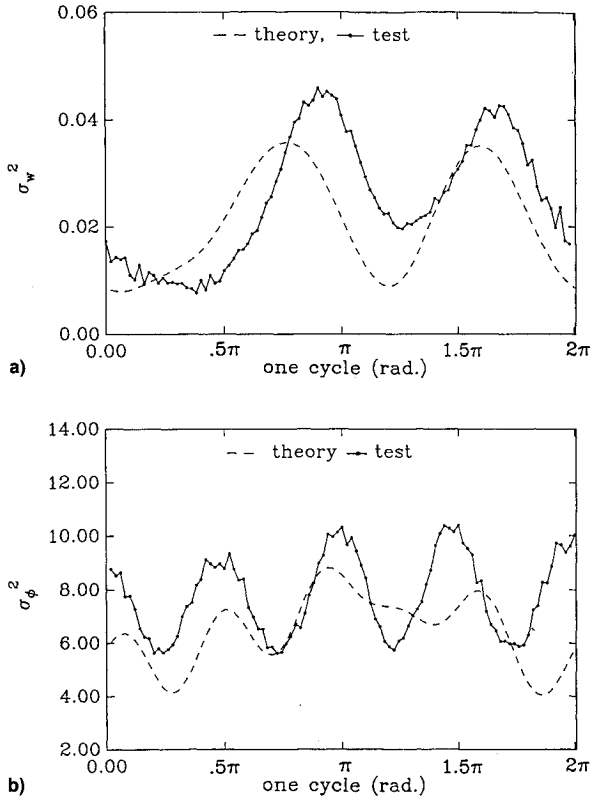

Fig. 11 Variance response for u_0 = 23 m/s, y_p = 2 in., θ_0 = 5 deg, for a) σ_w^2 vs ψ and b) for σ_ϕ^2 vs ψ.

to Fig. 6b, the torsional variance change is evident. The primary reason is that there is a stronger second harmonic component (16 Hz) in the lateral gust generated by the no. 2 and no. 3 RSC/airfoils. This excitation component is near the first torsional natural frequency. The secondary reason is due to addition of the random component in the longitudinal gust at this θ_0.

V. Concluding Remarks

A new experimental method based on the RSC/airfoil gust generator and a nonrotating rotor blade model in a wind-tunnel environment has been developed to simulate the gust response of a rotating rotor blade in forward flight. The theoretical and experimental variance responses of the flapping and torsional motions, as functions of the azimuth position of a rotor blade under the excitations of the lateral and longitudinal turbulence, have been computed and compared to the experimental results. The results are very similar to those obtained from an actual helicopter in forward flight or a rotational blade model in the wind tunnel. The major advantages of the present experimental method are to simplify the configuration of an experimental model and also the relative convenience of the experimental measurement. This new experimental method is especially suitable for a small wind tunnel that is used to study aeroelastic problems of a rotor blade model. The principal limitation of this method is the lack of velocity variation along the blade span and the absence of the effect of the reversed flow region near the blade root.

The modified linear ONERA aerodynamic model is convenient for use in the direct simulation time domain method. The gust calculated response using this aerodynamic model is in reasonable agreement with the present experimental results.

Acknowledgments

This work was supported by the Army Research Office under Grant DAAL03-87-K-0023, Gary Anderson is the technical monitor. We thank Philip Bayly for his assistance with the gust control technique. All numerical simulations were done on the supercomputer, Cray Y-MP, in the North Carolina Supercomputing Center (NCSC), Research Triangle Park, North Carolina.

References

[1]Grant, B. E., "A Method for Measuring Aerodynamic Damping of Helicopter Rotor in Forward Flight," *Journal of Sound and Vibration*, Vol. 3, No. 3, 1966, pp. 407–421.

[2]Gaonkar, G. H., "Interpolation on Aerodynamic Damping of Lifting Rotors in Forward Flight from Measured Response Variance," *Journal of Sound and Vibration*, Vol. 18, No. 3, 1971, pp. 381–389.

[3]Kana, D. D., Yeakley, L. M., and Dalzell, J. F., "An Experimental Model for Studying Dynamic Responses of a Rotating Beam Under Spatially Distributed Random Excitation," *Experimental Mechanics*, Vol. 8, No. 9, 1968, pp. 385–396.

[4]Yasue, M., Vehlow, G. A., and Ham, N. D., "Gust Response and Its Alleviation for a Hingeless Helicopter Rotor in Cruising Flight," Fourth European Rotorcraft and Powered Lift Aircraft Forum, Paper 28, Stresa, Italy, Sept. 1978.

[5]Ham, N. D., Bauer, P. H., Lawrence, T. H., and Yasue, M., "A Study of Gust and Control Response of Model Rotor-Propellers in a Wind Tunnel Air Stream," NASA CR-137756, ASRL-TR-174-4, Aug. 1975.

[6]Reed, W. H., III, "Flutter Exciter," U.S. Patent 4,809,553, March 7, 1989.

[7]Takens, F., "Detecting Strange Attractors in Turbulence," *Lecture Notes in Mathematics*, Vol. 898, Springer-Verlag, Berlin, 1981, pp. 366–381.

[8]Tang, D. M., and Dowell, E. H., "Response of a Nonrotating Rotor Blade to Lateral Turbulence Part I: Theory," *Journal of Aircraft*, Vol. 32, No. 1, 1995, pp. 145–153.

[9]Tang, D. M., Katz, A., and Dowell, E. H., "An Experimental Investigation of a Rotating Slotted Cylinder Gust Generator in a Wind Tunnel," *Journal of Fluid and Structures* (to be published).